Stability and evolution of a dry spot

P. G. López, M. J. Miksis, and S. G. Bankoff

Citation: Physics of Fluids **13**, 1601 (2001); doi: 10.1063/1.1369607
View online: http://dx.doi.org/10.1063/1.1369607
View Table of Contents: http://scitation.aip.org/content/aip/journal/pof2/13/6?ver=pdfcov
Published by the AIP Publishing

Stability and evolution of a dry spot

P. G. López,[a] M. J. Miksis, and S. G. Bankoff
McCormick School of Engineering and Applied Science, Northwestern University, Evanston, Illinois 60208

(Received 16 November 2000; accepted 15 January 2001)

The motion of a thin viscous layer of fluid on a horizontal solid surface bounded laterally by a dry spot and a vertical solid wall is considered. A lubrication model with contact line motion is studied. We find that for a container of fixed length the axisymmetric equilibrium solutions with small dry spots are unstable to axisymmetric disturbances. As the size of the dry spot increases, the equilibrium solutions become unstable to nonaxisymmetric disturbances. In addition, we present numerical solutions of the nonlinear evolution equations in the axisymmetric and nonaxisymmetric cases for different values of the parameters. The axisymmetric results show good agreement with existing experimental results. © *2001 American Institute of Physics.* [DOI: 10.1063/1.1369607]

I. INTRODUCTION

The nonhomogeneous deposition of a liquid over a solid surface often leads to the formation of dry spots. Examples can be found in a wide variety of situations, some of which are very familiar, as in the pouring of oil from the side of a saucepan, or the trapping of air bubbles when applying paint to a surface. Others, appearing in industrial processes involving the coating of a solid surface, are not as familiar. Further evolution of the system is a matter of substantial importance. In particular, the dynamics of the boundary of the dry spot, the contact line, is of considerable interest.

Equilibrium solutions for the profiles of axisymmetric systems have been well documented since the early works of Lamb[1] and Padday.[2] In a theoretical and experimental study of axisymmetric holes in liquid films, Taylor and Michael[3] showed that when the film sheet extends to infinity, an equilibrium solution which is energetically unstable exists for a film of thickness less than some critical value. Sharma and Ruckenstein[4] showed that, for a given contact angle in a finite domain, two isochoric holes of different radius are feasible. Using an energy argument, they showed that the thicker film is unconditionally stable while the other is unstable. These static analyses imply that any hole larger than the unstable one will open up and smaller holes will close. Moriarty and Schwartz[5] considered the evolution of an axisymmetric hole on a finite domain in the lubrication limit. They found an equilibrium solution and performed a numerical study of the evolution of the fluid profile, in which numerical slip was introduced at the moving contact line. It was found that a particular hole with an initial radius slightly larger than the corresponding unstable static solution, but with a higher surface energy, can actually close instead of opening, as predicted by the static studies.

We will develop a lubrication model for the motion of a fluid film on a horizontal solid surface bounded laterally by a dry spot and a vertical solid wall. The lubrication approximation yields a nonlinear evolution equation for the liquid–gas interface. The size of the dry spot is identified with the contact line, where some special considerations must be taken into account. When the usual no-slip boundary condition is used at the solid surface a force singularity appears at the contact line (see Ref. 6). To remove this singularity, a Navier slip condition with a singular slip function is used along the solid. This condition was first used by Greenspan,[7] and more recently by Haley and Miksis,[8] when modeling the motion of a drop on a solid surface, and by López *et al.*[9] in their investigation of nonisothermal spreading over an inclined plane. As the liquid spreads over the solid, a relationship between the observed dynamic contact angle and the velocity at the contact line is assumed. Relations of this type have been the subject of numerous theoretical (Blake,[10] Dussan,[11] and Hocking[12]) and experimental studies (Schwartz and Tejeda,[13] Hoffman,[14] and Dussan *et al.*[15]). They have been used in different spreading problems by Greenspan,[7] Ehrhard and Davis,[16] Hocking[17] and more recently by McKinley *et al.*[18] among others. Good agreement with experiment has been found in the study of nonisothermal drop spreading (Ehrhard[19]) and the investigation of spreading over an inclined plane (López *et al.*[20]). A common feature of this type of relationship is the appearance of a parameter [D in Eq. (18)] that depends on the interaction between the solid, the liquid, and the gas at the contact line, and which gives a measure of the mobility of the contact angle. For large values of this parameter (see Sec. II), an asymptotic solution can be determined where a quasiequilibrium state for the shape of the interface is established to leading order. This limit, first studied by Greenspan,[7] has received some confirmation in the experimental study of Ehrhard.[19]

Here we will perform a linear stability analysis on the axisymmetric equilibrium solutions found by Moriarty and Schwartz.[5] The linear theory confirms the results of the static analysis of Taylor and Michael[3] and Sharma and Ruckenstein.[4] For a given volume and static contact angle, the axisymmetric solution near the wall is stable and the one close to the axis of symmetry is unstable. In the limit when

[a]Present address: División de Física Aplicada, CICESE, Ensenada, B. C. 22860, México.

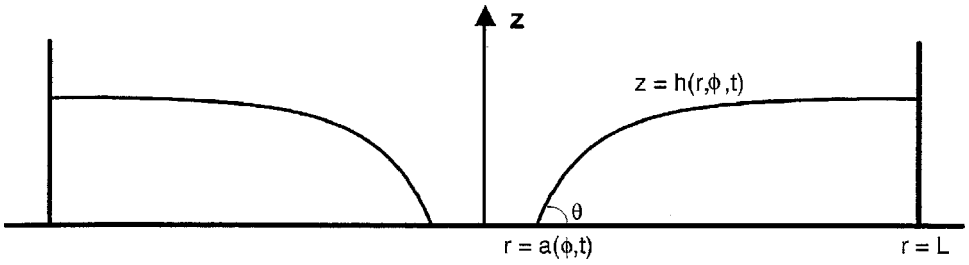

FIG. 1. Geometry of a liquid sheet bounded laterally by a dry spot at $r=a(\phi,t)$ and a vertical wall at $r=L$.

the radius of the vertical wall goes to infinity, the stable solution is lost, and the radius of the unstable solution goes to infinity. In this case holes of all sizes are unstable to axisymmetric disturbances. The linear analysis also shows that static solutions are always unstable to the first asymmetric mode. This mode dominates the instability in the quasisteady-state limit ($D\to\infty$) for solutions close to the wall, where higher order modes also become unstable. The higher-order asymmetric modes become the dominant mode of instability for these ''large solutions'' when the full problem is considered (finite D case).

In addition, the nonlinear system is studied. First we consider the axisymmetric case. Here the system is solved numerically for both the complete system and the quasisteady-state limit. Predictions for the radial position and velocity of the contact line, as well as the shape of the interface, are made for different values of the parameters. The quasisteady-state limit is found to predict well the global dynamics of the system in the limit of large contact line mobility D. We present evolution results in this limit, with the parameters given by the physical values of the experimental study of Diez *et al.*[21] Finally, numerical solutions are found for the three-dimensional evolution of nonaxisymmetric holes in the quasisteady limit. The numerical simulations show that small perturbations of circular contact lines grow, causing the dry spot to move closer towards the wall. In one case ''fingering instabilities'' are observed in the wetting region close to the axis. These instabilities are similar to the wetting instabilities observed in the spreading of liquid films over solid surfaces, which have been well documented by Huppert,[22] Silvi and Dussan,[23] Troian *et al.*,[24] Hocking and Miksis,[25] and López *et al.*,[9,20] among others.

II. FORMULATION

We consider an incompressible, viscous thin liquid film in contact with a solid surface located at $z=0$. Cylindrical polar coordinates (r,ϕ,z) are used, with the corresponding velocity field $\mathbf{u}=(u,v,w)$. The liquid film is bounded laterally by a dry spot located at $r=a(\phi,t)$ and a solid wall at $r=L$. The liquid–gas interface is located at $z=h(r,\phi,t)$. A cross section is shown in Fig. 1.

In order to apply the lubrication approximation we need to introduce dimensionless variables. We will keep the same notation for the dimensionless variables as introduced above. First define a capillary length

$$l=\sqrt{\sigma_0/\rho g} \tag{1}$$

as the radial length scale. Here σ_0 and ρ are the surface tension and density of the liquid, respectively, while g denotes the acceleration due to gravity. Next let h_0 denote the characteristic vertical length and define a lubrication-type parameter appropriate for thin films: $\varepsilon=h_0/l\ll 1$. The dimensionless hydrodynamic equations and boundary conditions are then expressed as a perturbation series in ε. To leading order in ε, the nondimensional Navier–Stokes and continuity equations are given by

$$-3\frac{\partial p}{\partial r}+\frac{\partial^2 u}{\partial z^2}=0, \tag{2}$$

$$-\frac{3}{r}\frac{\partial p}{\partial \phi}+\frac{\partial^2 v}{\partial z^2}=0, \tag{3}$$

$$1+\frac{\partial p}{\partial z}=0, \tag{4}$$

$$\frac{1}{r}\frac{\partial}{\partial r}(ru)+\frac{1}{r}\frac{\partial v}{\partial \phi}+\frac{\partial w}{\partial z}=0. \tag{5}$$

In the above equations, the velocities parallel to the plate, u and v, have been scaled with

$$U_0=\frac{\sigma_0 h_0^3}{3\mu l^3}, \tag{6}$$

where μ is the viscosity of the liquid, while the vertical component of the velocity w has been scaled with $U_0\varepsilon$. The scale for the pressure field p is $\rho g h_0$ and l/U_0 is the time scale.

At the liquid–gas interface $z=h(r,\phi,t)$, we have the kinematic boundary condition

$$w=\frac{\partial h}{\partial t}+u\frac{\partial h}{\partial r}+\frac{v}{r}\frac{\partial h}{\partial \phi}, \tag{7}$$

plus the conditions that the stresses balance in the normal and tangential direction,

$$p=\nabla^2 h, \tag{8}$$

$$\frac{\partial u}{\partial z}=\frac{\partial v}{\partial z}=0. \tag{9}$$

At the liquid–solid interface $z=0$, the vertical component of the velocity is zero:

$$w=0, \tag{10}$$

and a Navier-type condition with a singular slip function is imposed

$$u-\frac{\lambda}{h}\frac{\partial u}{\partial z}=0$$

and

$$v-\frac{\lambda}{h}\frac{\partial v}{\partial z}=0, \tag{11}$$

where λ is the slip coefficient scaled with h_0^2.

The lubrication system (2)–(11) is solved in the usual way to obtain a nonlinear evolution equation for the liquid–gas interface $h(r,\phi,t)$:

$$h_t+\frac{1}{r}\frac{\partial}{\partial r}\{(h^3+3\lambda h)rP_r\}+\frac{1}{r^2}\frac{\partial}{\partial \phi}\{(h^3+3\lambda h)P_\phi\}=0, \tag{12}$$

where the subscripts denote partial derivatives, and P is given by

$$P=\nabla^2 h-h=h_{rr}+\frac{1}{r}h_r+\frac{1}{r^2}h_{\phi\phi}-h. \tag{13}$$

This term expresses the competition between capillary and gravitational forces.

Additional conditions need to be specified at the leading edge of the dry spot, $r=a(\phi,t)$. Here the liquid makes contact with the solid surface

$$h=0, \tag{14}$$

and forms a contact angle θ with the solid. The contact angle is the angle the film interface makes with the solid surface $z=0$, in the plane perpendicular to $z=0$, and containing the normal vector to the contact line. Scaling the contact angle with ε, to leading order the scaled contact angle is given by

$$\theta=h_r\left(1+\frac{a_\phi^2}{a^2}\right)^{1/2}. \tag{15}$$

In the model presented here, a relationship between the normal velocity of the contact line U_s and the contact angle θ is assumed. Much experimental and theoretical work has been done to determine the exact form of the θ vs U_s curve (Schwartz and Tejeda,[13] Hoffman,[14] Blake and Haynes,[10] Ehrhard,[19] among others). In all of these investigations the value of the reported contact angle is found to be a monotonic increasing function of the velocity at the contact line. In addition an interval $I=[\theta_R,\theta_A]$ is found with the property that if $\theta\in I$ the contact line does not appear to move. This is known as contact angle hysteresis. We choose to ignore contact angle hysteresis ($\theta_R\to\theta_A$) here, and use a somewhat general relationship which in dimensional form (overbar variables) is given by

$$\overline{U_s}=\frac{\varpi\sigma_0}{3\mu}(\overline{\theta}^m-\overline{\theta_s}^m). \tag{16}$$

Here ϖ is a positive constant that depends only on the solid–liquid–gas interaction, and not the liquid or solid properties of either one alone, and $\overline{\theta_s}$ is the static (advancing or receding) contact angle. The exponent $m=1$ follows from the model derived by Blake and Haynes[10] when the changes in the contact angle are small compared with the static value (Greenspan[7]). The value $m=3$ is suggested by the studies of Schwartz and Tejeda[13] with a value of $\varpi\sim 1/13$ and the experimental data of Hoffman,[14] where $1/25\lesssim\varpi\lesssim 1/13$. The exact value of ϖ is not relevant for the analysis presented here. A similar law that is only a function of the difference between the contact angle and its static value, $\overline{U_s}=\kappa(\overline{\theta}-\overline{\theta_s})^m$, has been used in numerous theoretical works of spreading.[9,19,26] The value of $m=3$ was tested experimentally by Ehrhard[19] in his investigation of drop spreading. Nevertheless, Hocking[27] pointed out that a relation like the one given by Eq. (16), with $m=3$, is a better fit to the data given by Hoffman[14] and recovers Tanner's Law. We should note that the experiments report an apparent contact angle (see, e.g., Dussan,[11] Kistler[28]). The actual contact angle is in a region of molecular dispersion, and cannot be measured. As in other works of contact line motion,[7,8,16,25] we will assume that the actual contact angle behaves similarly to the apparent.

When dimensionless variables are introduced into (16), assuming a small static contact angle $\overline{\theta_s}=\varepsilon$ and using (15), the leading order in ε boundary condition at the contact line becomes

$$a_t=\frac{1}{D}\left(1+\frac{a_\phi^2}{a^2}\right)^{1/2}\left(1-h_r^m\left[1+\frac{a_\phi^2}{a^2}\right]^{m/2}\right). \tag{17}$$

Here $a_t(1+a_\phi^2/a^2)^{-1/2}$ is the normal velocity of the contact line, which is positive when the film is receding and negative when the film is advancing. The dimensionless parameter D measures the mobility of the contact line, and is given by

$$D=\frac{\varepsilon^{3-m}}{\varpi}. \tag{18}$$

The aim here is the study of the region near the dry spot, rather than the effects of the contact line formed at the vertical wall $r=L$, but conditions still need to be specified there. The wall is modeled as a solid into which there is no penetration. If the vertical wall has the same physical properties as the horizontal solid plate, then the static angle that the liquid makes with the wall would be equal to $\overline{\theta_s}$. This small angle is not desirable for the purposes of the present analysis. Instead, a static value of $\pi/2$ is assumed (i.e., a flat film). This value permits a comparison with previous works (see, for example, Moriarty and Schwartz[5]) and it is also the natural boundary condition for the case when the fluid sheet extends to infinity. In the dynamic case, the corresponding contact angle versus contact line velocity relation is one in which contact angle variations are small compared with the static value. Therefore, the leading order boundary conditions at the solid wall $r=L$ can be written as

$$h_r=0, \tag{19}$$

$$P_r=0. \tag{20}$$

The dimensional volume is given by $\overline{V_0}=2\pi l^3\overline{\theta_s}V_0$, where V_0 is

$$V_0=\frac{1}{2\pi}\int_0^{2\pi}\int_{a(\phi,t)}^{L} rh(r,\phi,t)\,dr\,d\phi. \tag{21}$$

Since the liquid is incompressible, this quantity is conserved by the evolution system (12)–(13), (14)–(17), (19)–(20). Therefore condition $V_0=$ const. holds for all times and is not imposed as a separate condition when the whole evolution equation (12) is considered. When we consider the limiting case of $D\to\infty$, this volume condition needs to be enforced.

In the large D limit a quasisteady state is established for all time (cf. the work of Greenspan[7]). The scaled time

$$\tau=\frac{t}{D}, \tag{22}$$

is introduced into the evolution equation (12) and into the condition at the contact line (17). An expansion in powers of $1/D$ is then performed. To leading order in $1/D$, the time derivative drops from the evolution equation and a solution for P is given by an arbitrary function of scaled time, $F(\tau)$. The problem then reduces to solving the spatial equation:

$$P=F(\tau), \tag{23}$$

in $r\in(a(\phi,\tau),L)$; $\phi\in(0,2\pi]$, subject to conditions (14) and (19) where the function $F(\tau)$ needs to be determined. The moving boundary is determined by back-substituting into (17) the value of the radial derivative at the contact line and using the condition $V_0=$ const. Note that the solution to the quasisteady problem can also be interpreted as an outer solution in time, in terms of the slow time τ. This limit, introduced by Greenspan[7] and used in several studies of drop spreading (see for example Ehrhard and Davis,[16] Haley and Miksis,[8] and Anderson and Davis[26]) defines a state of equilibrium of capillary and gravitational forces for the shape of the interface, where the leading edge is advanced via the contact angle versus contact line velocity relation. An order D^{-2} correction to the axisymmetric drop spreading problem can be found in the work of Greenspan and McKay.[29] Also note that the parameter D^{-1} is not a capillary number, but instead a parameter that depends on the liquid–solid–gas interaction at the contact line. It does not depend on the properties of the liquid or solid alone. This follows directly from the contact angle versus contact line velocity studies of Schwartz and Tejeda[13] and Hoffman[14] among others, as pointed out by Hocking.[27]

The evolution equation (12) subject to conditions (14)–(17) and (19)–(20) must be complemented by a choice of initial conditions. The solution to this nonlinear evolution system in terms of the two parameters, D and L, determines completely the solution to our lubrication model for the spreading of a thin liquid sheet bounded laterally by a dry spot and a vertical solid wall.

III. LINEAR STABILITY OF AXISYMMETRIC STATIC SOLUTIONS

The axisymmetric equilibrium solutions of the lubrication system (12)–(13), (14)–(17), (19)–(20) are found by solving

$$\frac{d}{dr}\left\{(h_0^3+3\lambda h_0)r\frac{dP_0}{dr}\right\}=0, \tag{24}$$

$$P_0(r)=\frac{d^2h_0}{dr^2}+\frac{1}{r}\frac{dh_0}{dr}-h_0, \tag{25}$$

for $a_0<r<L$, plus the boundary conditions at the contact line $r=a_0$,

$$h_0=0$$

and

$$\frac{dh_0}{dr}=1, \tag{26}$$

and the conditions at the vertical wall $r=L$

$$\frac{dh_0}{dr}=0$$

and

$$\frac{dP_0}{dr}=0. \tag{27}$$

The static solution was found by Moriarty and Schwartz[5] in terms of modified Bessel functions of the first kind:

$$h_0(r)=\frac{I_1(L)[K_0(r)-K_0(a_0)]+K_1(L)[I_0(r)-I_0(a_0)]}{I_1(a_0)K_1(L)-K_1(a_0)I_1(L)}. \tag{28}$$

The scaled volume is given by

$$V_0=\left(\frac{a_0^2-L^2}{2}\right)\frac{K_1(L)I_0(a_0)+K_0(a_0)I_1(L)}{I_1(a_0)K_1(L)-K_1(a_0)I_1(L)}-a_0. \tag{29}$$

Moriarty and Schwartz plotted the volume as a function of a_0 for a given value of L and different values of the contact angle. These plots show the existence of a maximum critical volume V_c that guarantees the existence of static solutions. In this case it is relevant to consider the critical volume V_c only as a function of L, since the contact angle has been scaled out. These plots show that for a given value of L there are two static isochoric solutions for a volume less than the critical value V_c, obtained at the critical value $a_0=a_c$, and a single static solution when the volume attains the critical value. The value of a_c is found when a_0 satisfies

$$a_0h_0''(a_0)+\left(\frac{a_0^2-L^2}{2}\right)\left(1-\frac{h_0''(a_0)}{a_0}-(h_0''(a_0))^2\right)=0. \tag{30}$$

In Fig. 2 we plot the height of the interface at the wall $h_0(L)$ for a hole of radius a_c as a function of L. As $L\to\infty$, $h_0(L)\to 1$, which in dimensional form is $\bar{h}_0(\bar{L})=l\bar{\theta}_s=\sqrt{\sigma_0/\rho g}\bar{\theta}_s$ as $\bar{L}\to\infty$, the small-angle result of Lamb.[1] In this limit the solution closer to the wall is lost and the static solution in the whole domain is given by

$$h_0(r)\to\frac{K_0(a_0)-K_0(r)}{K_1(a_0)}. \tag{31}$$

We now determine the linear stability to three dimensional disturbances of the basic state h_0, given by Eq. (28). Let the free surface $h(r,\phi,t)$ and the leading edge $a(\phi,t)$ suffer small increments from their static values $h_0(r)$ and

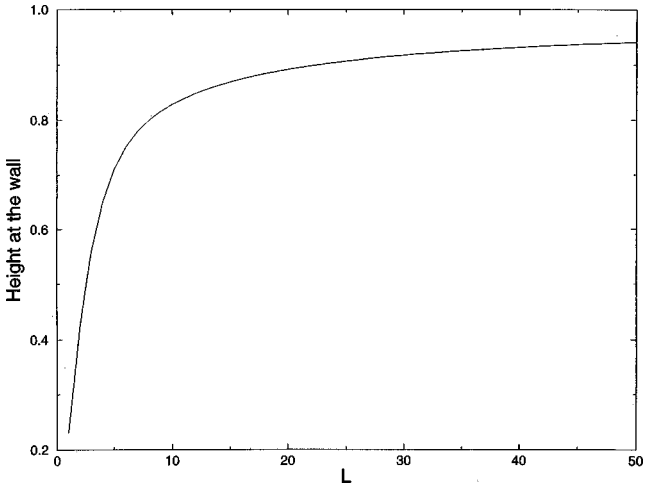

FIG. 2. Equilibrium height at the wall as a function of L for holes with $a_0=a_c$.

a_0. We obtain the equations for the perturbations by neglecting powers of δ higher than the first when we substitute into Eq. (12) the dependent variables

$$a(\phi,t)\to a_0+\delta a_1\exp\{\sigma t+i\ q\phi\}, \tag{32}$$

$$h(r,\phi,t)\to h_0(r)+\delta h_1(r)\exp\{\sigma t+i\ q\phi\}, \tag{33}$$

and collect $O(\delta)$ terms. Here the perturbations have been expressed in terms of normal modes with the wave number q taking integer non-negative values. The resulting linear equation is

$$\sigma h_1+\frac{1}{r}\frac{d}{dr}\left\{(h_0^3+3\lambda h_0)r\frac{dP_1}{dr}\right\}-\frac{q^2}{r^2}(h_0^3+3\lambda h_0)P_1=0, \tag{34}$$

where P_1 denotes

$$P_1(r)=\frac{d^2h_1}{dr^2}+\frac{1}{r}\frac{dh_1}{dr}-h_1\left(1+\frac{q^2}{r^2}\right). \tag{35}$$

The corresponding boundary conditions for the linear problem at the contact line are

$$h_1(a_0)=-a_1$$

and

$$h_1'(a_0)=\left[\frac{\sigma D}{m}+h_0''(a_0)\right]h_1(a_0). \tag{36}$$

At the wall the boundary conditions are given by

$$h_1'(L)=0$$

and

$$P_1'(L)=0. \tag{37}$$

Note that the volume constraint is automatically satisfied for $q\neq 0$. For $q=0$ volume is conserved as a limit of the linear equation (34) unless $\sigma=0$ (or $D\to\infty$), in which case we must impose the volume condition

$$\int_{a_0}^{L} rh_1dr=0. \tag{38}$$

In general, the eigenvalues σ and the eigenfunctions h_1 in the linear problem (34)–(37) could be complex. Here we will show that they are real. First note that Eq. (34) can be written as $-L[h_1]=\sigma h_1$ and then take the inner product of this equation with rP_1:

$$\langle -L[h_1],rP_1\rangle=\langle \sigma h_1,rP_1\rangle. \tag{39}$$

We see that the left hand side of (39) is a positive real number independent of σ since

$$\langle -L[h_1],rP_1\rangle=\int_{a_0}^{L}[h_0^3+3\lambda h_0]\left[r\|P_1'\|^2+\frac{q^2}{r}\|P_1\|^2\right]dr, \tag{40}$$

where $\|\ \|$ denotes the complex norm. The right hand side of (39) yields

$$\langle \sigma h_1,rP_1\rangle=-\frac{D\|\sigma a_1\|^2a_0}{m}-\sigma\|a_1\|^2a_0h_0''(a_0)-\sigma\int_{a_0}^{L}r\left[\|h_1'\|^2+\|h_1\|^2\left(1+\frac{q^2}{r^2}\right)\right]dr. \tag{41}$$

Equations (39)–(41) imply that the eigenvalues are real. Note that the eigenfunctions of the unstable modes (σ positive) satisfy the relation

$$\left\{\|h_1(a_0)\|^2a_0h_0''(a_0)+\int_{a_0}^{L}r\left[\|h_1'\|^2+\|h_1\|^2\left(1+\frac{q^2}{r^2}\right)\right]dr\right\}\leqslant 0. \tag{42}$$

We can determine the eigenvalues and eigenfunctions of the quasisteady approximation $\overline{\sigma}=D\sigma$ $(D\to\infty)$. For the axisymmetric mode $q=0$, these are given by

$$\overline{\sigma}=\frac{m[(L^2-a_0^2)(a_0-h_0''(a_0)-a_0(h_0''(a_0))^2)-2a_0^2h_0''(a_0)]}{L^2+a_0^2+a_0h_0''(a_0)(L^2-a_0^2)}, \tag{43}$$

and the corresponding eigenfunctions by

$$h_1(r)=C\left[\frac{2a_0}{L^2-a_0^2}+\frac{I_0(r)K_1(L)+K_0(r)I_1(L)}{I_1(a_0)K_1(L)-K_1(a_0)I_1(L)}\right], \tag{44}$$

where C is a constant.

For $q\neq 0$ disturbances, the eigenvalues and eigenfunctions of the quasisteady approximation are

$$\overline{\sigma}=m\left\{\frac{\Phi_q[L]\Psi_q[a_0]-\Psi_q[L]\Phi_q[a_0]}{a_0[\Phi_q[L]I_q(a_0)+\Psi_q[L]K_q(a_0)]}-h_0''(a_0)\right\},$$

$$\Phi_q[x]=xK_{q-1}(x)+qK_q(x), \tag{45}$$

$$\Psi_q[x]=xI_{q-1}(x)-qI_q(x),$$

and

$$h_1(r)=C[\Phi_q[L]I_q(r)+\Psi_qK_q(r)]. \tag{46}$$

In Fig. 3 we plot the growth rate $\overline{\sigma}$ given by (43) and (45) as a function of the radius a_0, for $q=0$, 1, 2, 3, and $q=4$, with $L=1$, and $m=3$ fixed. The axisymmetric mode $q=0$, is unstable for radii lesser than certain value a_c, while

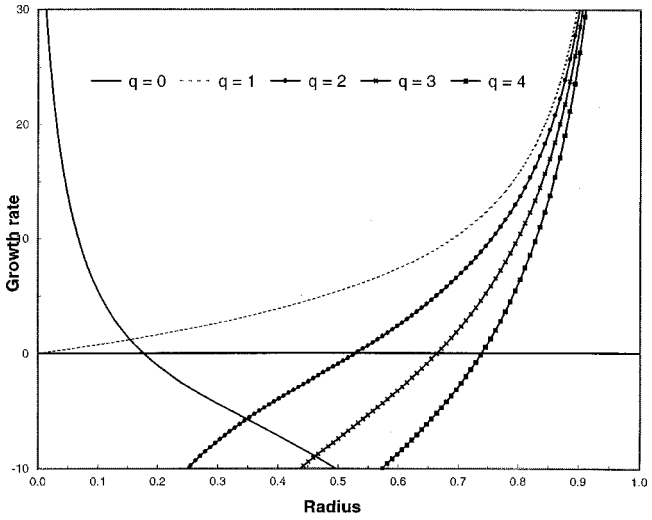

FIG. 3. Linear stability analysis in the quasisteady limit of $L=1$. Growth rate $\bar{\sigma}$ as a function of the radius of the hole a_0 for $q=0$, $q=1$, $q=2$, $q=3$, and $q=4$.

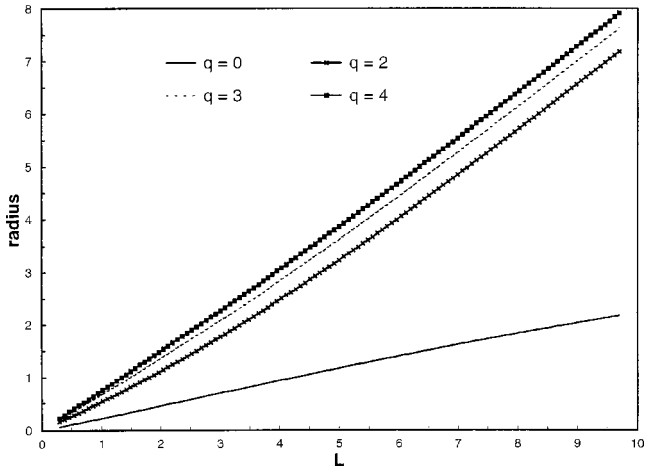

FIG. 5. Linear stability analysis for axisymmetric disturbances, in the quasisteady limit. Neutral stability curves as a function of L, for $q=0$, $q=1$, $q=2$, $q=3$, and $q=4$.

the static solution closer to the wall $a_0>a_c$ is stable. The $q=1$ mode is always unstable. When $0<a_0\lesssim 0.19$ the dominant mode is the axisymmetric one $q=0$. We observe that the $q=1$ mode dominates the instability for holes with $0.19\lesssim a_0<L=1$. For $q=2,3,4,...$, the solution with a radius smaller than the certain value $a_c^{(q)}$ is stable, and unstable for $a_0>a_c^{(q)}$.

In Fig. 4 the same plots are shown, but now the wall is located at $L=5$. A hole with an unstable proportional radius grows more slowly than in the $L=1$ case, for all values of the wave number. Hence, the neutral stability (where $\bar{\sigma}=0$) values a_c and $a_c^{(q)}$ increase. In Fig. 5, we plot these values as a function of the scaled length L for $q=0$, 2, 3 and $q=4$. Note that when the quasisteady approximation is neutrally stable, the finite D case is also neutrally stable. In the axisymmetric case $q=0$, this condition is the same condition for maximum volume given by Eq. (30). It follows that for a given L and a given volume $V<V_c$ the static solution closer to the wall $a_0>a_c$ is stable and the solution closer to the axis $a_0<a_c$ is unstable. For $L\to\infty$ all the solutions are unstable to axisymmetric disturbances since only the solution with $a_0<a_c$ exists. In this limit $q=1$ has $\sigma=0$ for all radii, while $q=2,3,4,...$ disturbances are all stable.

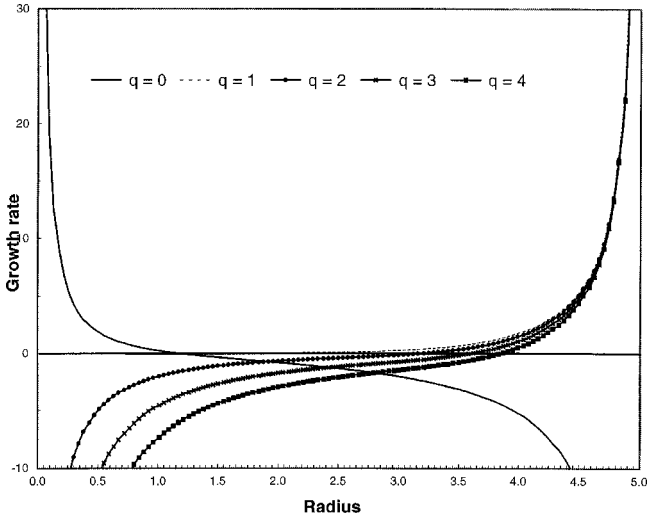

FIG. 4. Linear stability analysis for in the quasisteady limit for $L=5$. Growth rate $\bar{\sigma}$ as a function of the radius of the hole a_0 for $q=0$, $q=1$, $q=2$, $q=3$, and $q=4$.

The complete linear problem (34)–(37) is solved numerically by discretizing the linear equation and the boundary conditions using a Chebyshev collocation method[30] and using the routine ''hqr'' from Eispack for real upper Hessenberg matrices[31] to find the eigenvalues. In the following, we will fix $\lambda=10^{-3}$ and $m=3$ in all of our numerical calculations. Taking smaller values of λ does not appear to give results much different than this value, while it allows for a reasonable number of collocation points in our calculations. This is consistent with previous work.[9,20,25] We note that in Hocking and Miksis,[25] an asymptotic solution was found as $\lambda\to 0$ and the results were compared to large values of λ. Only a weak dependence in λ was observed in the stability results. Hence the results we present are only a function of the static radius a_0 and the parameters D and L. Note from Eq. (29) and our earlier discussion that for fixed L, the volume of the base state $h_0(r)$ varies with a_0, and this should be kept in mind when interpreting our stability results.

In Fig. 6 we take $D=1$ and $L=1$ and plot the value of the maximum growth rate σ as a function of the radius of the hole a_0 for $q=0$, 1, 2, 3 and $q=4$. As expected, the radius where the axisymmetric disturbance $q=0$ becomes stable is $a_0\approx 0.22$, which is also the radius a_c corresponding to the critical volume V_c given by (30). When $0<a_0\lesssim 0.21$ the dominant mode is the axisymmetric one $q=0$. We observe that the $q=1$ mode is unstable for a radius less than the value where the axisymmetric mode becomes stable. This mode dominates the instability for holes with $0.21\lesssim a_0\lesssim 0.575$. The next mode $q=2$ is dominant for holes with $0.575\lesssim a_0\lesssim 0.724$, and as the radius increases the higher modes will prevail, but the interval where a specific value of the wave number dominates narrows with q. Changing the

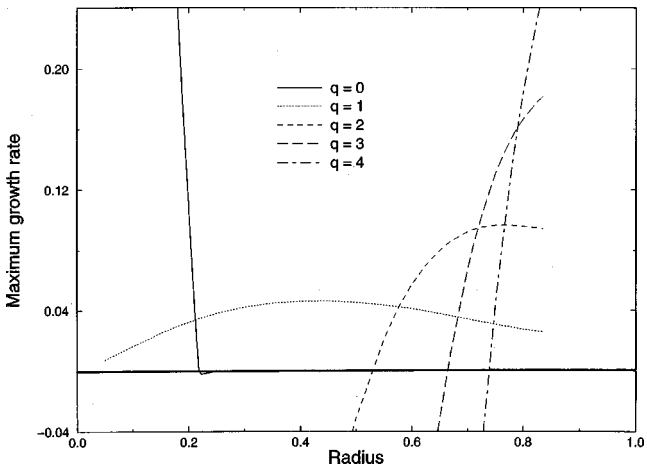

FIG. 6. Linear stability analysis for $L=1$. Maximum growth σ as a function of the radius of the hole a_0 for the wavenumbers $q=0$, $q=1$, $q=2$, $q=3$, and $q=4$.

value of the parameter D changes the value of the maximum growth rate, but the neutral stability radii (the values where $\sigma=0$) are independent of the parameter D, for all wave numbers.

IV. EVOLUTION OF AXISYMMETRIC HOLES

We now solve the nonlinear evolution equation in the axisymmetric case, i.e., we set $\partial/\partial\phi=0$ in the nonlinear system (12)–(13), (14)–(17), (19)–(20). Consider an equilibrium solution with radius a_0 and corresponding volume V_0. As initial conditions we take a function $H_0(r)$ of volume V_0 that satisfies the equilibrium equation (24), the condition at the wall (20), and makes contact with the horizontal surface at $\hat{a}_0=a_0+\delta$, where δ is a small number. The function $H_0(r)$ is not an equilibrium solution since $H_0'(\hat{a}_0)\neq 1$. When $a_0>a_c$, then $H_0'(\hat{a}_0)>1(<1)$ for $\delta>0(<0)$. In this case, the solution just closes (opens) to the stable solution at a_0 as predicted by the linear stability analysis performed in the previous section. In the unstable case when $a_0<a_c$ the opposite occurs and must be investigated in more detail. We will consider first two distinctive cases with $a_0=0.1$: (i) holes initially opening ($\delta=0.005$) and (ii) holes initially closing ($\delta=-0.005$). From (17) we see that the initial velocity at the contact line is given by

$$v_{\text{init}}=\frac{[1-(H_0'(\hat{a}_0))^3]}{D}. \tag{47}$$

Consider for the moment the quasisteady case. As noted earlier, in this limit we are left to solve a spatial equation (23), which in the axisymmetric case is an ordinary differential equation (ODE). Applying the condition of contact (14) and the condition (19), we find that the interface h is given by

$$h(r,\tau)=G_1(\tau)[K_1(L)(I_0(r)-I_0(a))+I_1(L)(K_0(r)-K_0(a))], \tag{48}$$

where the function G_1 is found by applying conservation of volume:

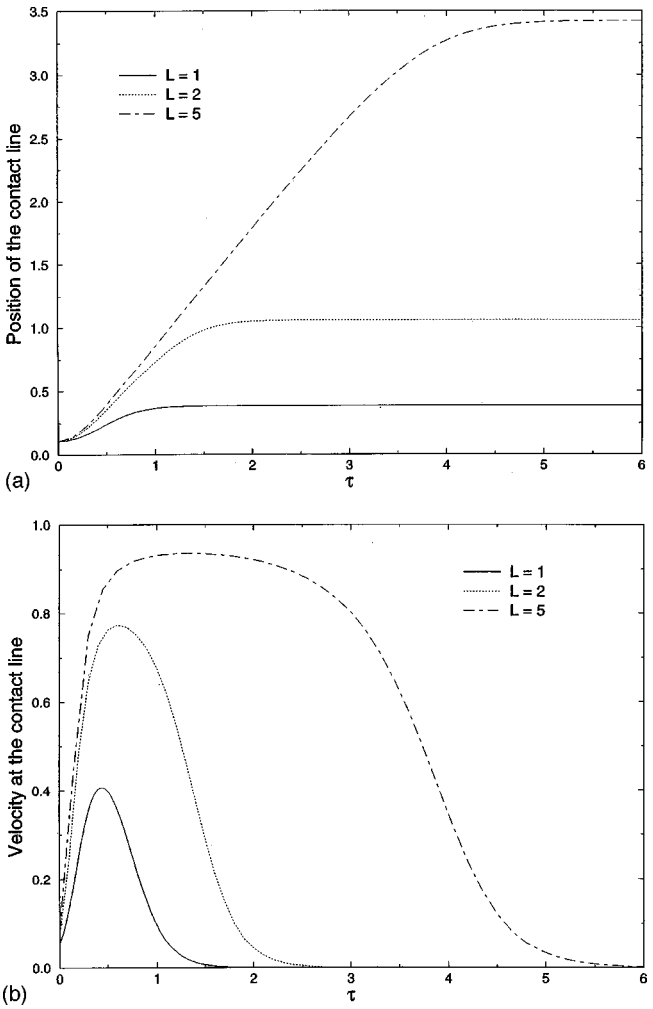

FIG. 7. Holes opening in the quasisteady limit for $L=1$, $L=2$, and $L=5$: (a) radial position of the leading edge $a(r,\tau)$; (b) radial velocity of the leading edge a_τ.

$$G_1(a(\tau))=V_0\left[\left(\frac{a^2-L^2}{2}\right)(K_1(L)I_0(a)+I_1(L)K_0(a))-aG_2(a)\right]^{-1}, \tag{49}$$

$$G_2(a)=K_1(L)I_1(a)-I_1(L)K_1(a). \tag{50}$$

Substituting the radial derivative of h at the contact line into the relation (17), the position of the dry spot is found by solving the ODE

$$a_\tau=1-[G_1(a)G_2(a)]^3. \tag{51}$$

Equation (51) can be easily integrated numerically. Note that the solution is independent of the slip coefficient λ. Results for the case of a hole initially opening (i) are shown in Figs. 7(a) and 7(b), where we plot the position of the contact line a and its radial velocity a_τ, respectively, for three different lengths $L=1(H_0'(\hat{a}_0)\approx 0.9816)$, $L=2(H_0'(\hat{a}_0)\approx 0.9743)$, and $L=5(H_0'(\hat{a}_0)\approx 0.9711)$. In all cases, the contact line accelerates until the velocity reaches a maximum and then decelerates until it smoothly reaches the stable solution close to the wall. From Fig. 7(b) we note that the initial velocity

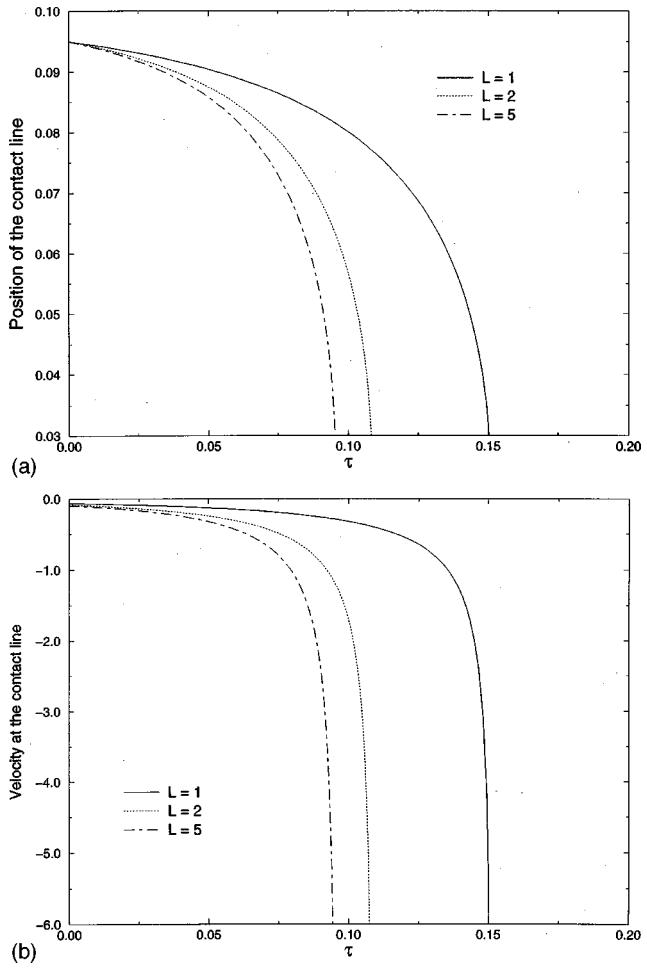

FIG. 8. Holes closing in the quasisteady limit for $L=1$, $L=2$, and $L=5$: (a) radial position of the leading edge $a(r,\tau)$; (b) radial velocity of the leading edge a_τ.

and the initial acceleration both increase with L. As the circular hole radius increases, a balance between gravitational and surface tension forces at the contact line is established. It starts to decelerate, with the mean deceleration slightly decreasing with L, since lengths have been scaled as the ratio of gravitational to capillarity effects. Note that for $L=5$ there is a region where the changes in the velocity are very small. The dynamics of a hole initially closing (case ii) are given in Figs. 8(a) and 8(b). Again we plot the radial position of the contact line a and its velocity a_τ, respectively, for the same set of lengths $L=1(H_0'(\hat{a}_0)\approx 1.0206)$, $L=2(H_0'(\hat{a}_0)\approx 1.028)$, and $L=5(H_0'(\hat{a}_0)\approx 1.0317)$. In these cases the initial velocity is negative. Again, it gets larger in magnitude as L increases. The initial state is slow, but is dominated by the contact line motion, so that forces are larger as L increases. As the hole gets smaller, it reaches a state where it collapses and finally closes.

For finite values of D the solution to the whole evolution system in the axisymmetric case must be solved numerically. We begin by introducing the following transformation for the independent variables

$$\xi=\frac{2L(a-r)}{r(L-a)}+1, \tag{52}$$

$$\Upsilon=t. \tag{53}$$

This maps the problem (12)–(13), (14)–(17), (19)–(20) into the domain $-1<\xi<1$ for $\Upsilon>0$. We discretize in space using a Chebyshev collocation method.[30] in $N+1$ collocation points ξ_j, $j=0,...,N$. The evolution equation is forced at the points ξ_j, $j=1,...N-2$ and the other three conditions are found by forcing (14), (19), and (20) to hold. We find it convenient to rescale the dependent variable as

$$\Omega(\xi,\Upsilon)=\frac{2L}{a(a-L)}h(r,t), \tag{54}$$

since this transformation makes changes at the contact line in the dependent variable independent of the position a. The result is a system of $N-2$ ODEs and two algebraic equations for the interface $\Omega_j(\Upsilon)=\Omega(\xi_j,\Upsilon)$, $j=1,...,N$. An extra ODE for the radius of the hole a is obtained from the contact angle vs slip relation (17). This differentio-algebraic system is then solved using the package DASSL.[32] Finally the system is retransformed to the original variables h, r, and t. The volume can easily be monitored at every time since we have the values of the interface at the Chebyshev collocation points. The conservation of volume serves as a check for our numerical method.

The evolution of the complete system is first examined for different values of the parameter D with $L=1$. In Figs. 9(a) and 9(b) we plot numerical results for the radial position and velocity of the contact line using the method described above when the dry spot is initially opening (i) for $D=0.1$, 1, 10. The global behavior is very similar to the quasisteady approximation where the solution opens to the stable solution. However, the initial stage of the hole is very different, since the initial velocity increases like D^{-1} [Eq. (47)]. For $t>0$ the front velocity instantaneously reaches a value to balance the surface and gravitational forces with the force at the contact line. Note that the jump from the initial data decreases with increasing D. This jump in the derivatives of h at the contact line has been described by Haley and Miksis.[8] The velocities and accelerations (positive and negative) decrease with increasing D. In Fig. 10, we plot the shape of the interface as the dry spot opens in time to the stable solution close to the wall, in a system with $L=1$ and for $D=1$. The results for the case where the dry spot is initially closing (ii) are shown in Figs. 11(a) and 11(b), where we again plot the radial position and velocity of the contact line for different values of D. As in case (i), velocities and accelerations decrease (in magnitude) with increasing D. The global behavior is again similar to the results for the quasisteady approximation. Solutions reach a point in time where surface tension forces along the contact line get very large, and the hole closes almost instantaneously.

The effects of increasing the length L for the full system are now investigated with $D=1$ fixed. In Fig. 12 we plot the radial position of the contact line for a hole that is initially opening (i). Two different positions of the vertical wall are considered: $L=1$ and $L=5$. For both cases, holes initially large with respect to the radius of the static solution open up to the other static solution. Increasing L increases the magnitude of the initial velocities and accelerations, just as in the

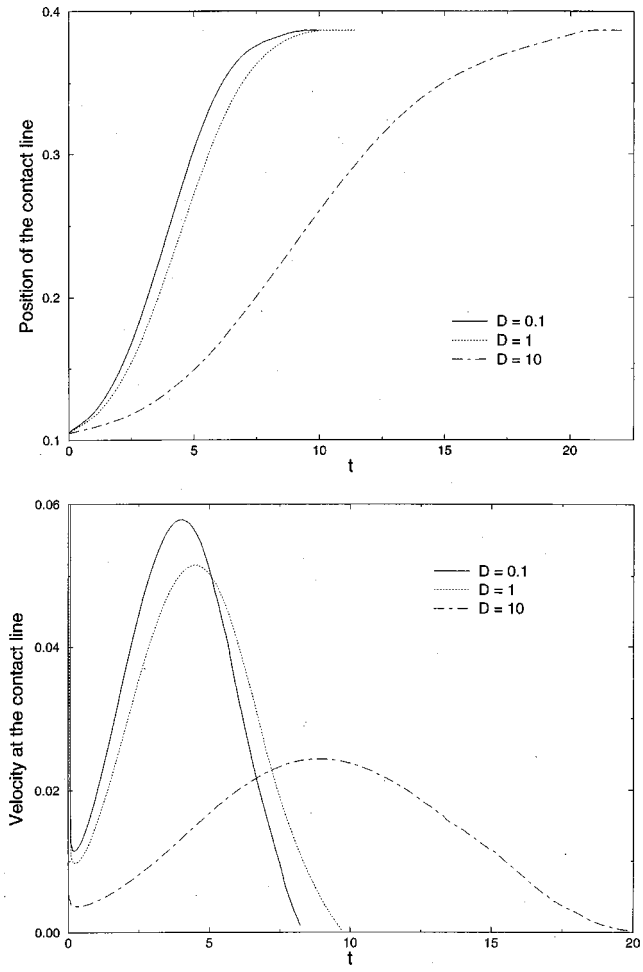

FIG. 9. Holes opening for $D=0.1$, $D=1$, and $D=10$, with $L=1$ fixed: (a) radial position of the leading edge $a(r,t)$; (b) radial velocity of the leading edge a_t.

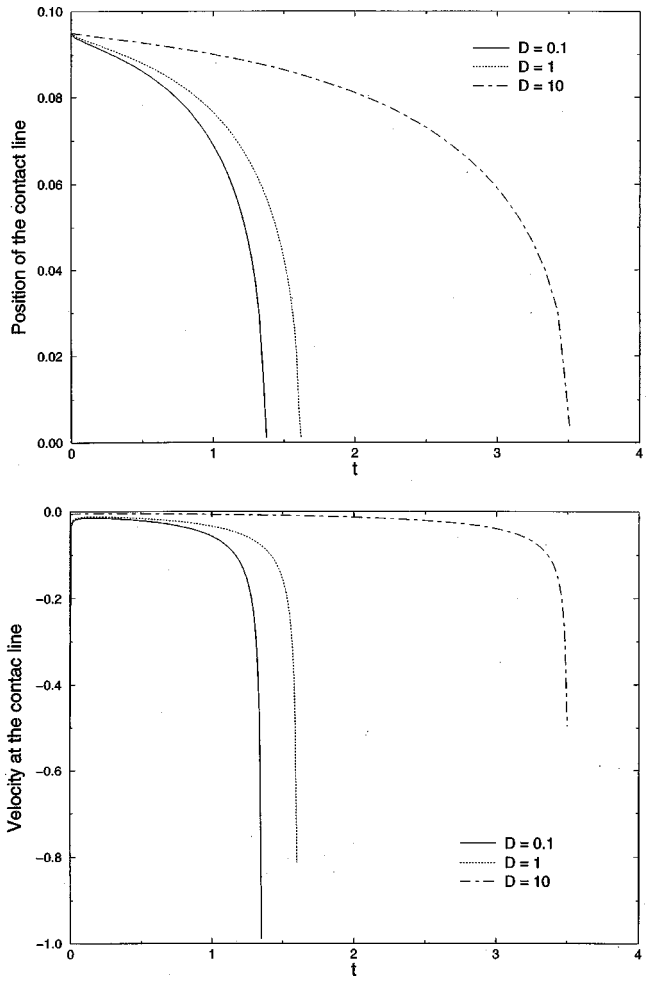

FIG. 11. Holes closing in a system with $L=1$ fixed, for $D=0.1$, $D=1$, and $D=10$: (a) radial position of the leading edge $a(r,t)$; (b) radial velocity of the leading edge a_t.

quasisteady case. A better comparison between the solutions for the quasisteady model and the model where changes in the shape are considered (finite D) is shown in Fig. 13 for a hole that has an initial radius larger than the equilibrium solution (i) in a system with $L=1$. In this figure the radial position of the contact line is plotted vs the scaled time $\tau = t/D$ in the quasisteady case and for $D=0.1$, 1 and $D=10$. It is clear that as we increase the value of the parameter D we recover the quasisteady results. From the studies of

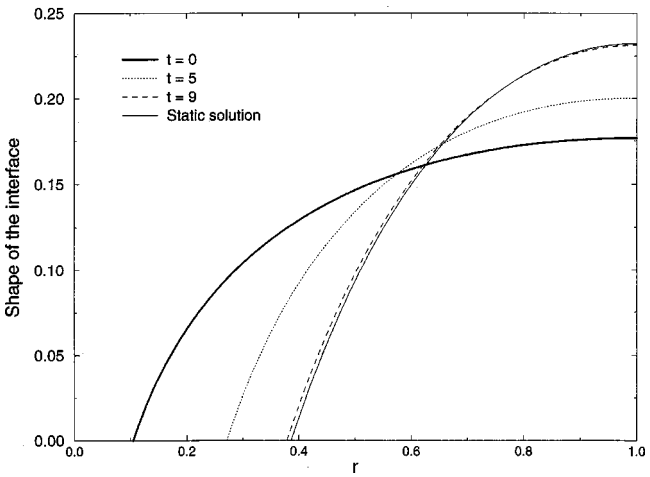

FIG. 10. Evolution of the shape of the interface $h(r,t)$ for a hole initially opening with $D=1$ and $L=1$.

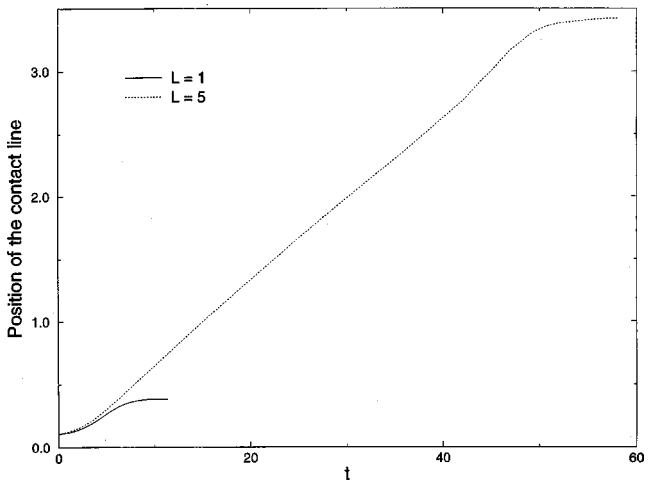

FIG. 12. Holes opening with $D=1$ in systems with $L=1$ and $L=5$. Radial position of the contact line $a(r,t)$.

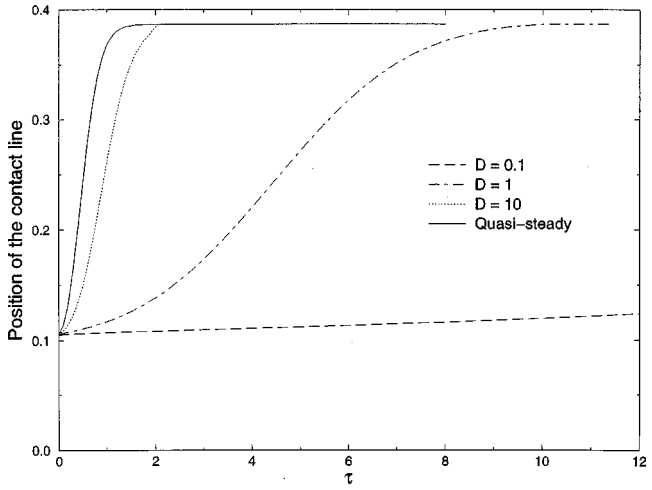

FIG. 13. Comparison between the quasisteady approximation and the finite D model for holes initially opening. Radial position of the contact line as a function of the scaled time $\tau = t/D$ for the quasisteady model and for $D = 0.1$, 1, and $D = 10$.

Schwartz and Tejeda[13] and Hoffman,[14] D is expected to be slightly larger than 10.

We now fix the parameters to the physical values corresponding to the experimental study of Diez *et al.*[21] In their experiment, a sheet of commercial silicone oil is originally placed in the annular region between two concentric radii $\overline{L} = 20$ cm and $\overline{a_0} = 5$ cm. The inner constraint is then removed and the fluid spreads over a solid surface made of Perspex, closing the dry region. In this experiment the static contact angle is zero, while the capillary length is $l = 0.15$ cm. In Fig. 14 we plot the dimensional position of the contact line $\overline{a}$ scaled with the inner radius $A = \overline{a}/\overline{a_0}$ versus the scaled time $T = (\tau_c - \tau)/\tau_c$, where τ_c is the time of closure. This plot corresponds to the experimental results shown

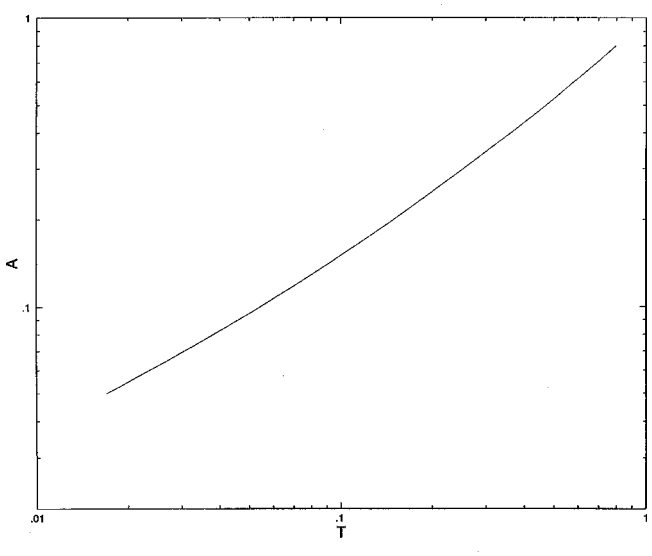

FIG. 14. Hole closing in the quasisteady limit for a physical system corresponding to the experimental study of Diez *et al.* (Ref. 20). Scaled position of the leading edge $A = \overline{a}/\overline{a_0}$, as a function of the scaled time $T = (\tau_c - \tau)/\tau_c$, where τ_c is the time of closure.

TABLE I. Value of the exponent α obtained by fitting the position of the leading edge $A = \overline{a}/\overline{a_0}$, as a function of the scale time $T = (\tau_c - \tau)/\tau_c$ (τ_c is the time of closure), to a power law: $\overline{a} \sim T^{\alpha}$, in the system studied by Diez *et al.* (Ref. 20).

Height at the vertical wall H_0 (mm)	Experimental exponent		Theoretical exponent
	Averaging four radii	Averaging area	
5	$\alpha = 0.710 \pm 0.007$	$\alpha = 0.781 \pm 0.003$	$\alpha = 0.783$
4	$\alpha = 0.785 \pm 0.005$	$\alpha = 0.776 \pm 0.004$	$\alpha = 0.769$
3	$\alpha = 0.734 \pm 0.006$	$\alpha = 0.783 \pm 0.086$	$\alpha = 0.751$
2	$\alpha = 0.833 \pm 0.006$	$\alpha = 0.626 \pm 0.006$	$\alpha = 0.727$

in Fig. (6) of the work of Diez *et al.*[21] This is done in the quasisteady approximation, i.e., we are solving the ODE:

$$a_\tau = -k[G_1(a)G_2(a)]^3, \tag{55}$$

where k is a positive constant accounting for the appropriate scaling factor. Therefore we are not concerned with the initial shape of the profile, the numerical value of the constant ϖ, or the initial height at the vertical wall H_0.

The curve fits the experimental data very well. The maximum deviation from a particular experimental point comes for the case that has an initial height at the vertical wall of $H_0 = 3$ mm at $T \approx 0.1$. This point is off by about 15% for the corresponding value of $\overline{a}$, but the curve hits the adjacent points corresponding to $H_0 = 5$ mm (the point to the right) and $H_0 = 4$ mm (the point to the left). Few experimental points are shown for a radius less than this value. Nevertheless, for radii greater than this value the maximum deviation from an experimental point is less than 5%. It is reported that for small radii they observed a larger deviation from circularity in the contact line. Therefore, the indirect measure of these points should have a greater experimental uncertainty. In the experiment the value of the radius is determined by two different methods: first, by averaging four orthogonal radii, and second by averaging the area free of oil. It is not reported which method was used in Fig. 6. In order to test the asymptotic behavior of the similarity solution obtained by Gratton and Minnoti,[33] they fitted the experimental values obtained by these two methods in the range $2H_0 \leqslant \overline{a} \leqslant 0.1\overline{L}$ to a power law: $\overline{a} \sim T^{\alpha}$. In Table I we compare these experimental values to the results of fitting the quasisteady results to a straight line, in the same ranges of $\overline{a}$. The experimental values of α corresponding to $H_0 = 5$ mm and $H_0 = 4$ mm, and using the second method, are consistent with Fig. 6. Hence, we again observe a good fit for these values by the quasisteady approximation. The value corresponding to $H_0 = 3$ mm and using the second method is also consistent with the values presented in Fig. 6. Now we can observe the relatively large experimental uncertainty. Considering this experimental uncertainty, our theoretical curve is again in the ranges of the experimental error. In their Fig. 6 no points are given for the small radii $H_0 = 2$ mm. For this value the predicted value of α is between the experimental values obtained with the two methods described above. On the other hand, the asymptotic behavior of T as $a \to 0$ can easily be found if we integrate the ODE and write it as

$$\tau = \int_{a_0}^{a} \frac{-k\,dx}{[G_1(x)G_2(x)]^3}$$

$$= \int_{a}^{0} \frac{k\,dx}{[G_1(x)G_2(x)]^3} + \int_{a_0}^{0} \frac{-k\,dx}{[G_1(x)G_2(x)]^3}. \tag{56}$$

The second integral in the right hand side is simply the closing time τ_c. Hence,

$$T = (\tau_c - \tau)/\tau_c$$

$$= \int_{0}^{a} \frac{dx}{[G_1(x)G_2(x)]^3} \Big/ \int_{a_0}^{0} \frac{dx}{[G_1(x)G_2(x)]^3}. \tag{57}$$

We can now integrate the first term of the convergent Taylor series in the integral

$$\int_{0}^{a} \frac{dx}{[G_1(x)G_2(x)]^3} = -\frac{L^6}{32} a^4 (\ln a)^3 + O(a^4(\ln a)^2), \quad a \to 0. \tag{58}$$

In the experiment the capillary length is relatively small. Therefore a small a regime might be difficult to report. Nevertheless, this asymptotic behavior as $a \to 0$ (58) suggests that fitting the experimental data to a power law might not be suitable for small radii.

The results shown to this point are consistent with the static results of Taylor and Michael[3] and Sharma and Ruckenstein[4] for thin films, but are taken from a dynamic point of view, with a contact line velocity versus contact angle relation built into it. We now examine an initial profile $\bar{H}_0(r)$ that is not a solution to the static equation in a system with $L=5$. This initial profile $\bar{H}_0(r)$ generates the same volume V_0 considered before, corresponding to a static solution with $a_0=0.1$. Initially the contact line is located at $\hat{a}_0 = 0.105$. The quasisteady approximation will immediately jump to an equilibrium profile with volume V_0, and since in this case $\hat{a}_0 > a_0$ it will open to the other equilibrium solution. However, in the finite D case the shape of the interface determines the velocity at the contact line for every instant in time. We take an initial profile in which $\bar{H}'(\hat{a}_0) \approx 1.55$. Consequently, the profile initially closes. In this case any equilibrium analysis fails to describe the dynamics of the dry spot. In Fig. 15 results for the shape of the interface $h(r)$ are shown for $D=1$ as the profile closes in time. This numerical example where an equilibrium analysis fails to predict the evolution is similar to the result of Moriarty and Schwartz.[5] However, we are able to predict the initial velocity at the contact line, since the model includes the dynamic relation at the contact line. As in their example, we can observe that the initial conditions cover a larger surface area than the static solution.

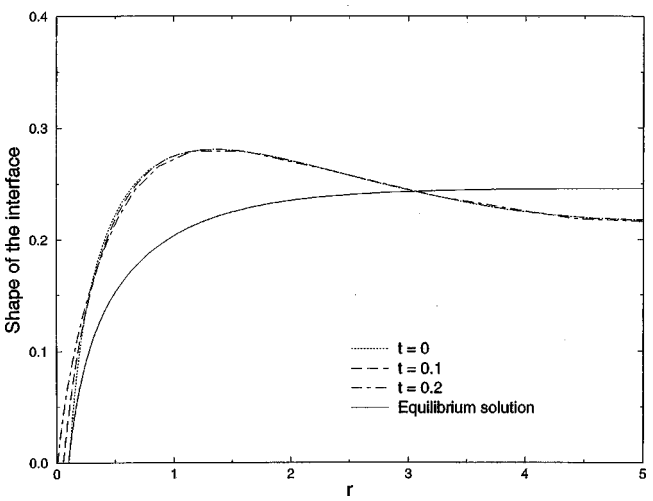

FIG. 15. Evolution of the shape of the interface $h(r,t)$ for a hole as it closes in time with $D=1$ and $L=5$. The initial conditions are not solutions to the equilibrium equation.

V. NUMERICAL EVOLUTION OF ASYMMETRIC HOLES

We now investigate the evolution of a dry spot that has no axial symmetry. Here we only present results using the quasisteady approximation. As shown in Sec. IV, we expect this to be a reasonable approximation of the solution for large values of D. In this limit we need to numerically solve the Helmholtz equation (23) coupled with the slip velocity versus contact angle relation (17), subject to the condition of contact (14) and the condition at the wall (20). As mentioned before, the condition of conservation of volume must be imposed as an extra condition.

Consider a dry spot determined by the equation

$$A(\phi) = a_0(1 + \delta \cos n\phi), \tag{59}$$

where $0 < a_0 < L$, n, and δ are constants. The initial profile $H(r,\phi)$ is a solution to

$$P = H_{rr} + \frac{1}{r} H_r + \frac{1}{r^2} H_{\phi\phi} - H = F_0, \tag{60}$$

in $r \in [A(\phi), L]\, \phi \in (0, 2\pi]$. The constant F_0 has the value that makes an axisymmetric hole of radius a_0 an equilibrium solution, i.e., if we take $\delta = 0$ in (59) then the initial profile H is a function of only r that satisfies the equilibrium system (24)–(27).

The spatial system (23), (28), (20) is solved numerically in terms of $a(\phi,\tau)$ and $F(\tau)$ using a Chebyshev–Fourier spectral collocation method that discretizes in the radial and angular direction, respectively. The radial coordinate is mapped into a fixed domain $\xi \in [-1,1]$ by the transformation

$$\xi = \frac{2L(r - a(\phi,\tau))}{r(a(\phi,\tau) - L)} + 1. \tag{61}$$

The discrete version of the spatial problem yields a linear system at the $NC+1$ Chebyshev collocation points for every one of the NF Fourier collocation points. These $NF \cdot (NC+1)$ linear equations are solved using a series of subroutines from the library LINPACK,[34] in terms of the position of the contact line at the NF Fourier points and the function F. The value of the radial derivative of the interface at the contact line is then substituted in the discrete version (in space) of the dynamic condition at the contact line (17). This determines a system of NF ODEs, which is then coupled with the

conservation of volume condition. This differentio-algebraic system is again solved using the self-adaptive package DASSL.[32] To find the shape of the interface h at a specific time τ we solve once more the linear system for the desired value of $a(\phi,\tau)$. The solution is completed when we return to the original variables.

In the following, we show numerical simulations for the nonaxisymmetric evolution of a dry spot in the quasisteady case, using the method described above for $m=3$. We first consider a system with $L=2$. In Figs. 16(a)–16(c) we take an initial profile $H(r,\phi)$, where the dry spot $A(\phi)$ has $n=1$, $a_0=0.9$, and $\delta=0.005$. In Fig. 16(a) we plot the contact line $a(\phi,\tau)$ as it evolves in time, while the time evolution of the contact line velocity a_τ as a function of the angle ϕ is shown in Fig. 16(b). The contact line and the contact line velocity are plotted at time intervals of $\Delta\tau=10$, starting at $\tau=0$. However, the final time is $\tau=198$ instead of $\tau=200$. This final time is the final time at which we obtained numerical convergence when we checked integer values of τ. As we approach this final computational time, the radial derivative of the interface at $\phi=0$ decreases considerably, but is not exactly zero. Obviously, our numerical method is not equipped to perform a followup into the breaking regime. From these figures we see that almost half of the liquid film does not cover the horizontal plate, as the contact line moves away from the axis of symmetry. The rest wets the horizontal solid plate as it approaches the axis of symmetry. At the beginning this wetting is uniform. But as the dry region approaches the vertical wall, this uniformity is lost and velocities increase in magnitude at the poles. In the final stages higher angular modes start to appear very quickly in the poles. This situation causes a fingering instability to appear close to the axis. This kind of instability has been well documented in the wetting of an inclined plane by liquid films, since the works of Huppert[22] and Silvi and Dussan[23] and more recently by Troian *et al.*[24] Hocking and Miksis[25] and López *et al.*[9,20] among others. At the end, a ''foot'' shape for the dry region is attained, while the film close to the wall is very dry, as can be observed in Fig. 16(c), where we show a surface plot of the liquid–gas interface at the final computational time $\tau=198$.

In Figs. 17(a)–17(c) we show the same plots for a system with $L=1$. In this numerical simulation the initial profile $H(r,\phi)$ has a dry spot $A(\phi)$ with $n=2$, $a_0=0.6$, and $\delta=0.005$. Again, we plot at time intervals of $\Delta\tau=10$, starting at $\tau=0$. In this case the final computational time is $\tau=91$ instead of $\tau=90$. In this simulation, the dry spot moves in two directions, while the wetting occurs only at the poles. From the evolution plots of the slip velocity versus ϕ we observe how the final stages are again characterized by the appearance of the higher angular modes in the wetting region. Again, the dry spot moved initially in the direction of the maximum perturbation and velocities increase in magnitude as time evolves. In Fig. 17(c) we show a surface plot of the liquid–gas interface for the final computational time $\tau=91$. It shows again the climbing of the liquid film on the container in the wetting region. In this case the final dry region is almost an ellipse.

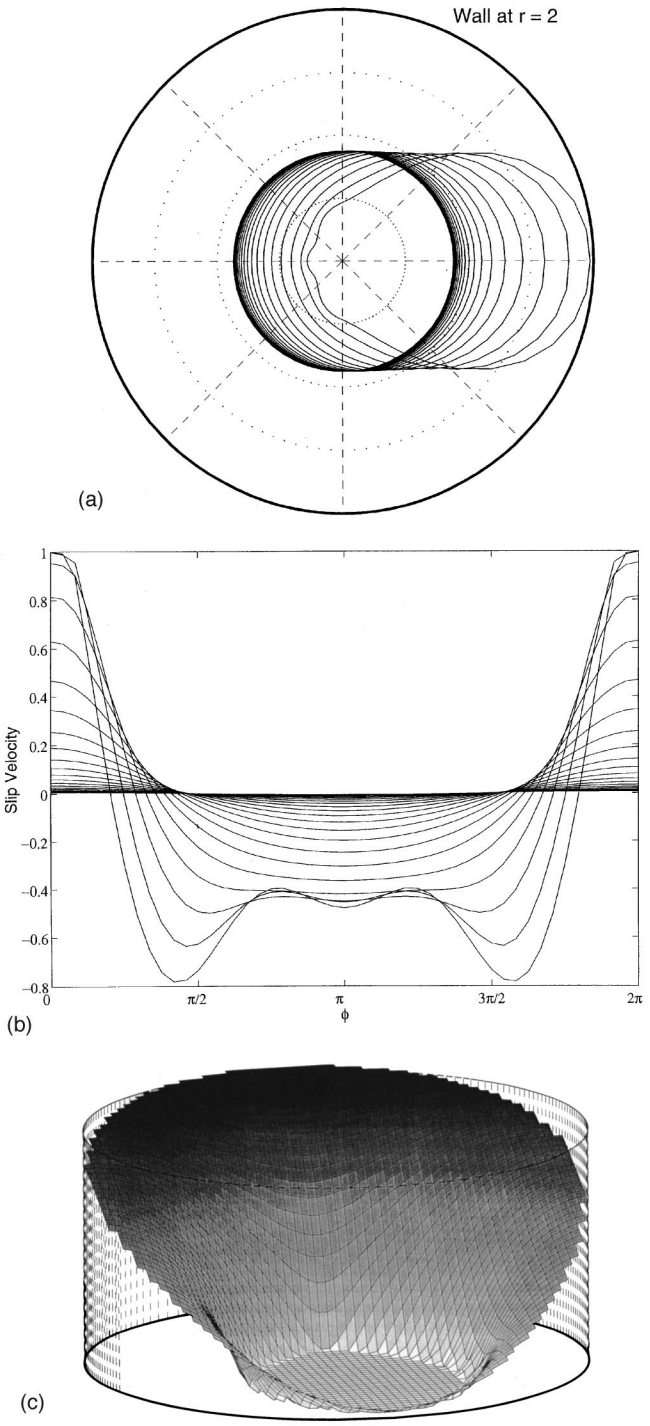

FIG. 16. Quasisteady evolution of a nonaxisymmetric hole in a system with $L=2$. Initially at $\tau=0$ the dry spot is given by $r=A(\phi)=0.9(1+0.005\cos\phi)$: (a) time evolution of the contact line $a(\phi,\tau)$; (b) time evolution of the contact line velocity at the contact line a_τ as a function of the angle ϕ. The time intervals in (a) and (b) is $\Delta\tau=10$. The final time is $\tau=198$ instead of $\tau=200$. (c) Shape of the interface $h(r,\phi,\tau)$ for the final time $\tau=198$.

VI. CONCLUSIONS

A lubrication model with contact angle variations for the dynamics of a sheet of fluid with a dry spot has been studied. The dynamics in the lubrication limit are described by a system composed of a nonlinear evolution equation for the

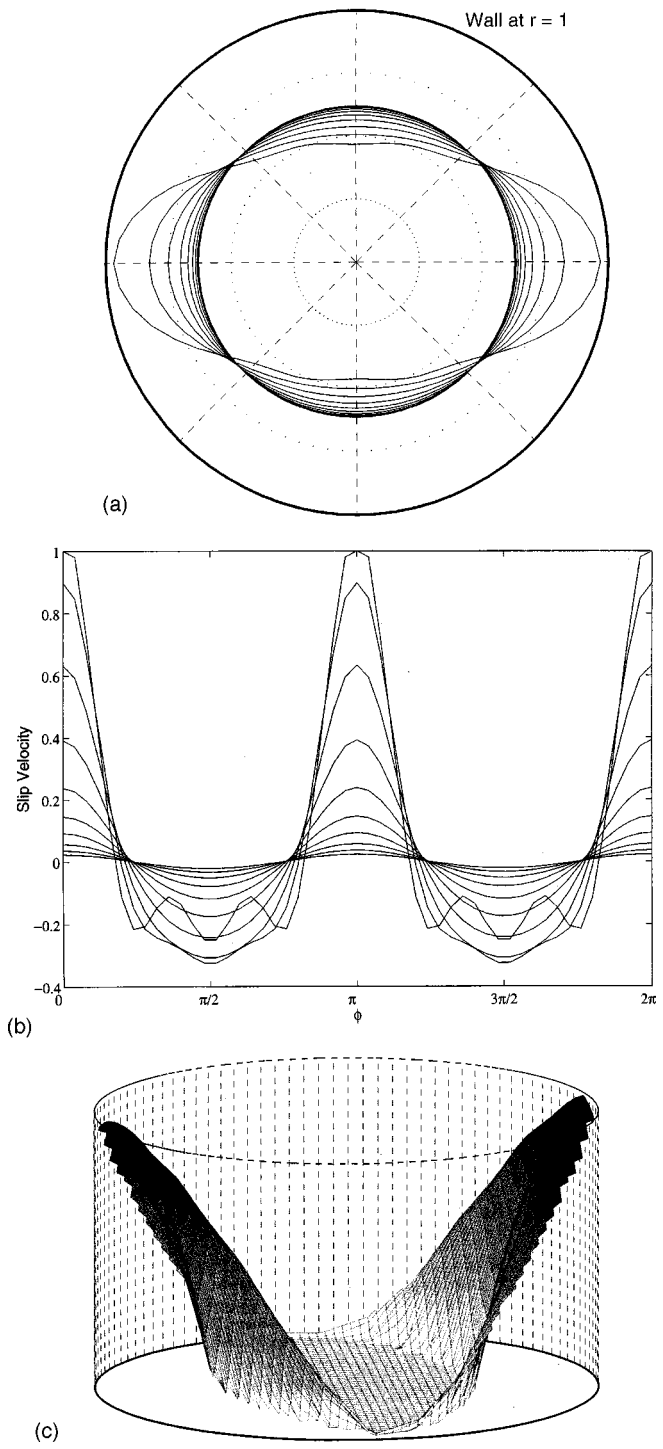

FIG. 17. Quasisteady evolution of a nonaxisymmetric hole in a system with $L=1$. Initially at $\tau=0$ the dry spot is given by $r=A(\phi)=0.6(1+0.005\cos 2\phi)$: (a) time evolution of the contact line $a(\phi,\tau)$; (b) time evolution of the contact line velocity at the contact line a_τ as a function of the angle ϕ. The time interval in (a) and (b) is $\Delta\tau=10$. The final time is $\tau=91$ instead of $\tau=90$. (c) Shape of the interface $h(r,\phi,\tau)$ for the final time $\tau=91$.

interface, and an equation describing the dynamics at the contact line owing to contact angle variations. The system contains two free parameters, which are the nondimensional position of the wall L, scaled with a capillary length, and a parameter appearing from the contact angle versus slip–velocity relation, denoted by D. The latter parameter is a function of the interaction between the solid, the gas, and the liquid at the contact line. As $D\to\infty$ a quasisteady state for the shape of the interface is established and the radius of the hole is determined as a solution to the equation for the contact angle versus contact line velocity equation in terms of the slow time $\tau=t/D$.

The equilibrium results of Taylor and Michael[3] and Sharma and Ruckenstein[4] are recovered. The three-dimensional linear stability analysis shows that static solutions close to the lateral wall are stable to axisymmetric disturbances, while those close to the axis of symmetry are unstable. This is in accord with previous results.[3–5] However, we found that static solutions are always unstable to the first asymmetric mode. As larger holes are considered, higher-order unstable modes appear.

The nonlinear system of equations has been solved numerically in the quasisteady state case and for the complete system for axisymmetric holes. Predictions for the radial position and velocity of the contact line, as well as the shape of the interface, were obtained for axisymmetric holes near the unstable solution. This study was done for different values of the scaled length L and the parameter D. Numerical simulations were performed first for holes that satisfy the static equation for the interface, but were initially to the right (left) of the unstable equilibrium position. These holes initially move away from the unstable equilibrium position. The holes to the right will open up to the stable equilibrium solution, while the holes to the left close up. When holes open the initial acceleration is large, followed by a region of small changes in the velocity. Then deceleration becomes large until the motion stops. For holes to the left, the initial movement is slow, but reaches a point where it suddenly closes. As the parameter D decreases velocities and accelerations increase. In the case where the initial conditions satisfy the equilibrium equation, the quasisteady limit $D\to\infty$ is a good approximation to the global behavior of the evolving contact line in the slow time scale. As the length of the system is increased, velocities and accelerations increase in magnitude. We found good quantitative behavior of the dynamic evolution in the quasisteady limit, upon comparing with the experimental study of Diez *et al.*[21] As in Moriarty and Schwartz,[5] we find that it is possible for dry spots to close when the initial radius is larger than the radius of the unstable static solution. In this special case, the quasisteady limit fails, since the profile immediately jumps to an equilibrium solution. Hence this approximation predicts that the hole opens. Here the initial movement dominates before the interface gets close to the equilibrium shape.

Finally, numerical investigations of the evolution of dry spots that have no axial symmetry were performed in the quasisteady limit. Dry spots that are initially noncircular were considered. The dry spots move to the side of the initial perturbation until it is almost dry, close to the vertical wall. In one case ''fingering instabilities'' are observed in the wetting region close to the axis.

ACKNOWLEDGMENTS

The authors are grateful to the referees that brought to their attention the experimental study of Diez *et al.*[21] This research was supported in part by NSF Grant No. CTS-9223464 and the US–Israel Binational Science Foundation, Grant No. 96-00395/2.

[1]H. Lamb, *Statics* (Cambridge University Press, Cambridge, 1916).
[2]J. F. Padday, ''The profiles on axially symmetric menisci,'' Philos. Trans. R. Soc. London **269**, 265 (1971).
[3]G. I. Taylor and D. H. Michael, ''On making holes in a sheet of fluid,'' J. Fluid Mech. **58**, 625 (1973).
[4]A. Sharma and E. Ruckenstein, ''Energetic criteria for the breakup of liquid films on nonwetting solid surfaces,'' J. Colloid Interface Sci. **137**, 433 (1990).
[5]J. A. Moriarty and L. W. Schwartz, ''Dynamic considerations in the closing and opening of holes in thin liquid films,'' J. Colloid Interface Sci. **161**, 335 (1993).
[6]E. B. Dussan V and S. H. Davis, ''On the motion of a fluid–fluid interface along a solid surface,'' J. Fluid Mech. **65**, 71 (1974).
[7]H. P. Greenspan, ''On the motion of a small viscous droplet that wets a surface,'' J. Fluid Mech. **84**, 125 (1978).
[8]P. J. Haley and M. J. Miksis, ''The effect of the contact line on droplet spreading,'' J. Fluid Mech. **223**, 57 (1991).
[9]P. G. López, S. G. Bankoff, and M. J. Miksis, ''Non-isothermal spreading of a thin liquid film on an inclined plane,'' J. Fluid Mech. **230**, 97 (1996).
[10]T. D. Blake and J. M. Haynes, ''Kinetics of liquid/liquid displacement,'' J. Colloid Interface Sci. **30**, 421 (1969).
[11]E. B. Dussan V, ''On the spreading of liquids on solid surfaces: Static and dynamic contact lines,'' Annu. Rev. Fluid Mech. **11**, 371 (1974).
[12]L. M. Hocking, ''Rival contact-angle models and the spreading of drops,'' J. Fluid Mech. **239**, 671 (1992).
[13]A. M. Schwartz and S. B. Tejada, ''Studies of dynamic contact angles on solids,'' J. Colloid Interface Sci. **38**, 359 (1972).
[14]R. L. Hoffman, ''A study of the advancing interface. I. Interface shape in liquid-gas systems,'' J. Colloid Interface Sci. **50**, 228 (1975).
[15]E. B. Dussan V, E. Ramé, and S. Garoff, ''On identifying the appropriate boundary conditions at a moving contact line: An experimental investigation,'' J. Fluid Mech. **230**, 97 (1991).
[16]P. Ehrhard and S. H. Davis, ''Non-isothermal spreading of liquid drops on horizontal plates,'' J. Fluid Mech. **229**, 365 (1991).
[17]L. M. Hocking, ''Spreading and instability of a viscous fluid sheet,'' J. Fluid Mech. **211**, 373 (1990).
[18]I. S. McKinley, S. K. Wilson, and B. R. Duffy, ''Spin coating and air-jet blowing of thin viscous drops,'' Phys. Fluids **11**, 30 (1999).
[19]P. Ehrhard, ''Experiments on isothermal and non-isothermal spreading,'' J. Fluid Mech. **257**, 463 (1993).
[20]P. G. López, M. J. Miksis, and S. G. Bankoff, ''Inertial effects on contact line instability in the coating of a dry inclined plate,'' Phys. Fluids **9**, 2177 (1997).
[21]J. A. Diez, R. Gratton, and J. Gratton, ''Self-similar solution of the second kind for a convergent viscous gravity current,'' Phys. Fluids A **4**, 1148 (1992).
[22]H. E. Huppert, ''Flow and instability of viscous gravity currents down a slope,'' Nature (London) **300**, 427 (1982).
[23]N. Silvi and E. B. Dussan V, ''On the rewetting of an inclined solid surface by a liquid,'' Phys. Fluids **28**, 5 (1985).
[24]S. M. Troian, E. Herbolzheimer, S. A. Safran, and J. F. Joanny, ''Fingering instabilities of driven spreading films,'' Europhys. Lett. **10**, 25 (1989).
[25]L. M. Hocking and M. J. Miksis, ''Stability of a ridge of fluid,'' J. Fluid Mech. **247**, 157 (1993).
[26]D. M. Anderson and S. H. Davis, ''The spreading of volatile liquid droplets on heated surfaces,'' Phys. Fluids **7**, 248 (1995).
[27]L. M. Hocking, ''On contact angles in evaporating liquids,'' Phys. Fluids **7**, 2950 (1995).
[28]S. F. Kistler, ''Hydrodynamics of wetting,'' in *Wettability*, edited by J. C. Berg, Surfactant Science Series, Vol. 40 (Marcel Dekker, New York, 1993), p. 311.
[29]H. P. Greenspan and B. M. McCay, ''On the wetting of a surface by a very viscous fluid,'' Stud. Appl. Math. **64**, 95 (1981).
[30]C. Canuto, M. Y. Hussaini, A. Quarteroni, and T. A. Zang, *Spectral Methods in Fluid Dynamics* (Springer, New York, 1988).
[31]B. T. Smith, *Matrix Eigensystem Routines: Eispack Guide* (Springer, New York, 1976).
[32]L. R. Petzold, *A Description of* DASSL: A *Differential-Algebraic System Solver* (Sandia National Laboratories, Sandia, New Mexico, 1982).
[33]J. Gratton and F. Minotti, ''Self-similar viscous gravity currents: Phase plane formalism,'' J. Fluid Mech. **210**, 155 (1990).
[34]J. J. Dongarra, C. B. Moler, and G. W. Stewart, LINPACK Users Guide (SIAM, 1979).